Chemical Engineering Journal 165 (2010) 668–677

Contents lists available at ScienceDirect

Chemical Engineering Journal

journal homepage: www.elsevier.com/locate/cej

Numerical modeling of mass transport in microfluidic biomolecule-capturing devices equipped with reactive surfaces

Sina Jomeh, Mina Hoorfar*

University of British Columbia, 3333 University Way, School of Engineering, Kelowna, BC V1V 1V7, Canada

ARTICLE INFO

Article history:
Received 1 July 2010
Received in revised form 9 September 2010
Accepted 10 September 2010

Keywords:
Microfluidics
Mass transport
Surface reaction
Numerical modeling

ABSTRACT

This paper presents and compares three different designs including open-channel, circular-pillar and screen-plate microreactors for capturing and detection of biomolecules in a buffer liquid. In general, these capturing/detection devices consist of a flow cell containing one or several reactive surfaces loaded with ligand molecules. The critical issue in the design of an efficient device is the proximity of the biomolecules to the ligands in the capturing stage since the latter is immobilized on the reactive surface and the former is freely moving in the flow. The flow pattern and the geometry of the device are the key factors in this regard. The presented designs are numerically modeled and compared in terms of capture efficiency. Immersed biomolecules are assumed to behave like a continuum medium. The Navier-Stokes and convection–diffusion equations are solved in two dimensions and the concentration profile is obtained after a certain sampling period. The chemical reaction between the ligand and the biomolecule is included in the model through solving the reversible kinetic equation at the boundaries. Considering the level of performance, and ease of implementation, the screen plates are found to be the favourable option for the purpose of biomolecule removal. The effects of the change in the geometric parameters (i.e., the number of plates and reactive side preference) and physicochemical parameters (i.e., the diffusion constant, ligand surface density, and forward and backward reaction rates all combined in non-dimensional numbers) on the capture efficiency of the screen plates are thoroughly inspected and the corresponding results are plotted.

1. Introduction

Unique features of microfluidic devices have attracted researchers' interest in a wide range of disciplines including biochemistry and biotechnology [1,2]. Due to their miniaturized design, different functionalities including mixing, pumping, separation and reaction can be integrated in narrow channels on a tiny chip [3]. This helps to reduce the cost of mass production and the risk of contamination existing in conventional macroscale devices [4,5].

Microreactors are the essential constituent of microfabricated chips for many chemical and biotechnological applications. High surface-to-volume ratio (10,000–50,000 m^2/m^3) and fast rates of heat and mass transfer in such devices cause the reactions to be more efficient than the macroscale counterparts [6]. The large value of the heat transfer coefficient leads to a more uniform sample temperature which itself results in a better control of experimental conditions. Moreover, the small size and the high rates intensify the reactions, shorten the residence time and consequently favour having higher throughputs [7].

One of the common applications of microreactors is to separate a phase from a buffer liquid using the binding specificity between two reactants [8]. This idea, for instance, has been implemented in affinity chromatography to remove biological molecules from the liquid phase [9,10]. Surface plasmon resonance sensors (SPR) [11,12], high frequency quartz microbalance [13] and hollow cantilever-based biosensors [14] used for the study of adsorption kinetics are among the examples of the above application. All the cases mentioned here deal with a buffer liquid flowing through a microchannel and mass being transported to the labelled surfaces.

Microreactors are generally divided into heterogeneous and homogenous categories. In the homogeneous reactors, reaction takes place within the solution. Conversely, in the heterogeneous reactors, one of the reactants (ligand) is immobilized on a solid surface and the other reactant is brought close to the surface by the carrier fluid. The reactive surface can be incorporated in thin layers on boundaries (so-called open channels) or in packed-bed configurations within the flow domain [15]. Because of the very small size and low Reynolds number, the main mechanism in the open channels for the transport of the immersed reactant is diffusion [16]. Packed-bed designs, on the other hand, add the effect of convection

* Corresponding author. Tel.: +1 250 807 8804.
E-mail address: mina.hoorfar@ubc.ca (M. Hoorfar).

1385-8947/$ – see front matter © 2010 Elsevier B.V. All rights reserved.
doi:10.1016/j.cej.2010.09.056

and decrease the diffusion path through constructing the reactive surfaces against the flow and reducing the size of flow passages [17]. As a result, the capturing performance increases or alternatively, smaller chambers for the same throughput are required for fabrication.

Mass transport from the buffer liquid to the reactive surface and vice versa in microreactors can be considered as a subcategory of solute dispersion (including both convection and diffusion) with chemical reaction. In 1953, Taylor [18] found an approximate analytical solution for the traverse mean variables of the convection–diffusion equation for the dispersion of a solute inside a tube with laminar flow and impermeable walls. However, no reaction and interphase transport was considered. His work was modified by many researchers using other analytical methods to achieve higher order accuracy of the analytical solution [19–21]. Sankarasubramanian et al. [22] extended the particle dispersion problem to the interphase transport systems. He derived an analytical relation for the mean concentration of a solute inside a tube with first-order reactions at the walls. However, their solution was confined to the case of irreversible reaction. Barton [23] added a linear bulk reaction to the previous model of Sankarasubramanian et al. [22], obtained an asymptotic solution for larger dimensionless times and extended the solution for the flow reactors. Shapiro et al. [24] solved the convection–diffusion equation with the irreversible first-order kinetic equation and included the external forces exerted on the particles, and also position-dependent diffusivity and rate constants. Both Barton and Shapiro et al. used the Taylor's dispersion theory (analytical method) which provides no detailed information about the concentration profile throughout the domain.

Analytical solutions, although valuable to provide an in-depth insight, are limited to very simplified cases. Many researchers tried to solve the convection–diffusion equation in complex geometries with or without the homogenous/heterogeneous chemical reactions. Dutta et al. [25,26] analyzed the particle dispersion in pressure-driven flows in microetched channels for different shapes of cross sections. However, no chemical reaction was considered in their model. In 2003, Baroud et al. [27] numerically solved the diffusion–convection–reaction equations for the reactions happening between two species in the bulk flow of a T-shaped microchannel (homogeneous reaction) and compared the results with the experiment. They assumed the reaction was irreversible and neglected the second derivatives of the concentration along the channel. Wang et al. [28] conducted similar simulation inside a Y-shaped microchannel and investigated the effect of adding obstacles on improving the mixing. The obstacles were not reactive on the surface and were used only to enhance the convective transport and mixing. In 2006, Aoki et al. [29] compared the performance of microreactors for mixing of two species in the bulk flow with different channel cross sections (such as rectangular and triangular shapes) introducing two non-dimensional parameters representing the relative strength of reaction/diffusion and aspect ratio of mean diffusion length. Their work focused on the bulk reaction, and not the heterogeneous reaction with the reactors embedded in the domain. Full momentum and mass transport equations were solved by Gervais et al. [30] for the case of heterogeneous reactions on the boundaries of a rectangular microchannel reactive on either one or both sides. They analyzed the bulk concentration and surface saturation behaviour versus non-dimensional parameters of the problem. However, the geometry presented was an open channel, and no effort was made to develop a solution for the packed designs. Waghode et al. [31] presented a numerical model of ammonia decomposition on reactive surfaces of a parallel-plate channel and also a single reactive cylinder centrally located in a microchannel. They coupled the momentum and convection–diffusion–reaction equations with the energy equations and used a simplified sink term to represent the reaction rate at the surface. Nonetheless, they did not consider the reversible kinetic equation which more accurately describes the chemical reactions on the surface. Moreover, only a single cylinder was used to reduce the simulation cost while in today's microchips, packed designs of microreactors are favourable and mostly used in real microplants to increase the output rate.

There have been tremendous studies aimed at modelling of the particle dispersion problem coupled with chemical reaction. However, no detailed investigation and comparison of the performance of open-channel and packed-bed heterogeneous microreactors were found considering both convection–diffusion and reversible chemical reaction at the reactive surfaces. In this paper, a numerical model is presented to investigate three different assemblies of the reactive surfaces (open-channel as well as packed-bed designs) in a microchannel. In order to verify the model, first, Graetz problem is solved in a rectangular microchannel, and the results are compared to the analytical solutions available in the literature for the entrance and fully developed regions [32]. Then, the accuracy of the simulation to fit the available experimental data is examined [17]. Once it is verified, the numerical model is used to analyze each of the three designs and compare them in terms of capture performance.

The first objective of this work is to investigate the effect of the reactive surface configuration on the device performance. The first configuration considered here is a rectangular open channel. This design resembles the common flow chamber devices currently being used to study the kinetics of microorganisms inside buffer liquids [33,34]. The next two designs are alternative configurations in packed-bed forms; one with circular pillars and the other one with screen plates. The numerical model introduced in this paper is developed to explore superiorities of one design with respect to the others. After finalizing the geometry, the next objective is to study the effect of other design parameters. These parameters range from chemical properties (such as the ligand surface density and reaction rates) to geometric properties (like the number of plates). The effects of these parameters are inspected and explained for the selected geometry by means of non-dimensional numbers governing the problem of mass transport [30]. In summary, this paper is aimed at the comparison of some of the commonly used configurations of microreactors and performing an efficiency analysis along with a parametric study of the selected design. It is not intended to propose a generalized framework to optimize the microreactors for different design parameters as it is almost impossible to do due to the diversity of the parameters [30].

The paper is organized as follows: in Section 2, the theory of mass and momentum transport are presented and the non-dimensional numbers governing the problem are discussed. In Section 3, first, the Graetz problem is solved to verify the numerical model introduced in the paper against the exact solution. Then, experimental data obtained from the literature [17] are compared with the numerical results to investigate the viability of the model to apply to real conditions. The geometries and dimensions of the capturing devices are explained in detail in Section 4. In Section 5, the results are presented in two parts: the first part elaborates the performance of each microreactor. The second part investigates the parameters essential for the design process.

2. Theory

2.1. Momentum transport and continuity equations

The buffer liquid is assumed to flow through a rectangular microchannel at steady state in the absence of body forces like gravity. Two-dimensional incompressible Navier-Stokes equations are used along with the continuity equation to find the velocity profile

throughout the domain.

$$\nabla \cdot \mathbf{u} = 0 \tag{1}$$

$$\rho \mathbf{u} \cdot \nabla \mathbf{u} = -\nabla p + \mu \nabla^2 \mathbf{u} \tag{2}$$

In this equation, $\mathbf{u}$ is the velocity vector, p is the pressure, ρ is the density, and μ is the dynamic viscosity. The no-slip boundary condition is assumed at the walls. Constant velocity is specified at the inlet. The outlet is assumed to be at atmospheric pressure.

2.2. Mass transport equation

After the flow reaches the steady-state condition, the solute (the immersed reactant) is released at the inlet at a specific concentration (C_0), and it is monitored after a certain sampling time period. This solute is carried by the liquid and transported to the reactive surfaces through diffusion and convection. The transient two-dimensional mass transport equation which is solved inside the domain (neglecting the effect of external forces) is as follows:

$$\frac{\partial C}{\partial t} + \mathbf{u} \cdot \nabla C = D \nabla^2 C \tag{3}$$

where C is the solute concentration in the bulk, and D is the diffusion coefficient.

For the chemical reaction at the reactive boundaries, rates of adsorption and desorption of the solute are included in the problem through a concentration flux term. The kinetic equation of the chemical reaction is used to calculate this flux.

$$\frac{\partial C_s}{\partial t} = k_{on} C_{wall} (C_{s0} - C_s) - k_{off} C_s \tag{4}$$

In this equation, C_{s0} is the surface concentration of the ligand (referring to the total number of the free sites available for binding), C_s is the surface concentration of the bound reactant (referring to the number of the occupied sites), and C_{wall} is the concentration of the solute adjacent to the wall. k_{on} and k_{off} are forward and backward reaction rates, respectively.

At the outlet, the convective flux is specified as

$$\mathbf{n} \cdot (-D \nabla C) = 0 \tag{5}$$

in which $\mathbf{n}$ is the normal vector to the boundary. All other boundaries are insulated or symmetry, which means

$$\mathbf{n} \cdot (-D \nabla C + C\mathbf{u}) = 0 \tag{6}$$

For all of the equations, the change in the physical properties due to temperature variation is neglected.

2.3. Non-dimensional forms of the governing equations

Due to the diversity of the variables involved in the problem of dispersion–reaction, non-dimensionalization allows for understanding the impact of each term on the output. This helps to explain the results in a more systematic way. The dimensionless forms of the mass transport and reaction kinetic equations are presented here [30]:

$$\frac{\partial C^*}{\partial t^*} + \left(u^* \frac{\partial C^*}{\partial x^*} + v^* \frac{\partial C^*}{\partial y^*} \right) = \frac{1}{Pe^2} \frac{\partial^2 C^*}{\partial x^{*2}} + \frac{\partial^2 C^*}{\partial y^{*2}} \tag{7}$$

$$\frac{\partial C_s^*}{\partial t^*} = \varepsilon Da [C_{wall}^* (1 - C_s^*) - K_D C_s^*] \tag{8}$$

where

$$x^* = \frac{x}{hPe}, \quad y^* = \frac{y}{h}, \quad t^* = \frac{Dt}{h^2}$$

$$u^* = \frac{u}{u_{avg}}, \quad v^* = \frac{v}{u_{avg}}, \quad C^* = \frac{C}{C_0}, \quad C_s^* = \frac{C_s}{C_{s0}}$$

where x^* and y^* are the dimensionless coordinates and t^* is the dimensionless time. h is the characteristic length (the flow path width), u_{avg} is the average inlet velocity, Pe is Peclet number, Da is Damkohler number, ε is the relative adsorption capacity and K_D is the equilibrium dissociation constant [30]. Thus, the four main non-dimensional parameters governing the problem are

$$Pe = \frac{u_{avg} h}{D}, \quad \varepsilon = \frac{C_0 h}{C_{s0}}, \quad Da = \frac{k_{on} C_{s0} h}{D}, \quad K_D = \frac{k_{off}}{k_{on} C_0} \tag{9}$$

Peclet number is the ratio of the convection and diffusion strengths while Damkohler number is the relative strength of reaction at the surface and diffusion towards it. To compare the relative strengths of convection and reaction, $k_{on} C_{s0} l / Uh$ is used in which l is the length of the reactive area [30]. These numbers will be used later to interpret the patterns obtained from the numerical results.

3. Model verification

The verification of the numerical model is accomplished in two steps. In the first step, the model is verified against the exact solution of a simplified form of the mass transport equation (Graetz problem). In the second step, the numerical data obtained for the mass transport inside a rectangular microchannel is verified with the experimental data obtained from the literature [17] without considering any specific limitation or simplification.

3.1. Model verification against the exact solution

For very large Peclet numbers at the steady-state condition with no lateral velocity in y direction, Eq. (7) reduces to the so-called Graetz equation [30]

$$u^* \frac{\partial C^*}{\partial x^*} = \frac{\partial^2 C^*}{\partial y^{*2}} \tag{10}$$

This equation along with the simplified version of the boundary condition for mass flux leads to a set of equations which can be solved analytically. Here, only the final results for the non-dimensional bulk concentration are used. The details on the solution procedure are presented in [30]. Bulk concentration at each section of the channel is calculated from the following formula

$$C_b = \int_0^h C u \, dy \tag{11}$$

Solving the Graetz problem for a rectangular microchannel with only one reactive surface (Fig. 1(a)) gives the non-dimensional bulk concentration as follows [30]

$$C_{b,entrance}^* = \exp(-1.467 x^{*2/3}) \tag{12}$$

$$C_{b,fully\ developed}^* = \exp(-2.4304 x^*) \tag{13}$$

Eq. (12) is valid in the entrance region while Eq. (13) is more accurate within the fully developed region. COMSOL Multiphysics software is used to model the mass and momentum transport (i.e., Eqs. (1)–(3)) inside the microchannel for $Pe = 50$ and $Da \to \infty$. The Navier-Stokes and the convection–diffusion equations are assumed to be decoupled. This assumption applies to the dilute solutions with no effect of the solute on the flow pattern. Thus, the Navier-Stokes equation is first solved to obtain the steady-state velocity profile inside the channel. Then, the convection–diffusion equation is solved to find the concentration profile. The result is presented in Fig. 1. The range of the non-dimensional parameters considered here is expected to yield a solution close to the Graetz problem. As it is shown in Fig. 1(b), the data points satisfactorily follow the entrance-model curve for smaller values of x^* and the fully

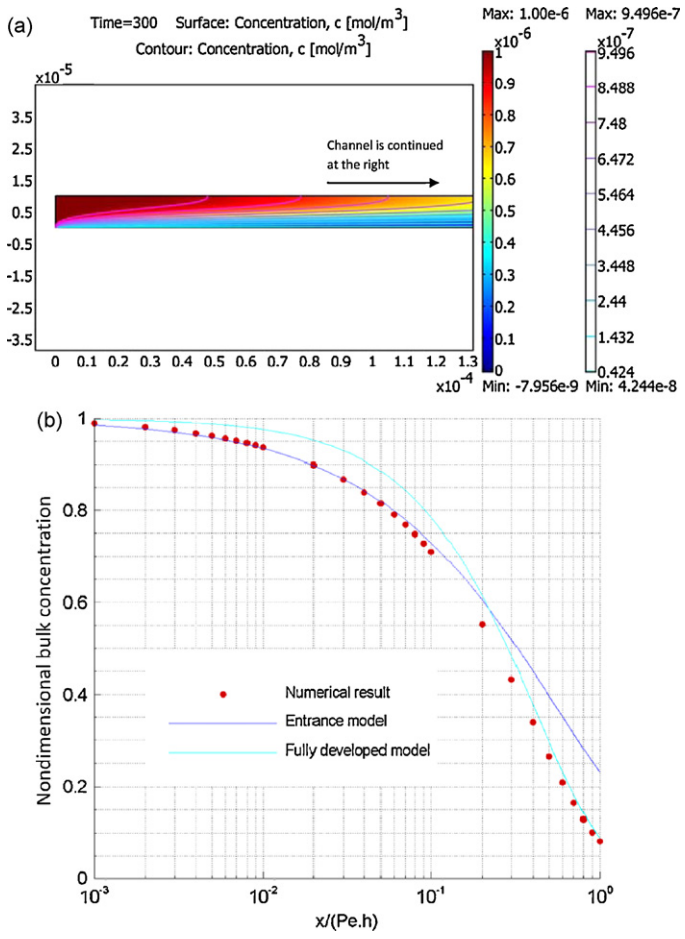

Fig. 1. (a) Rectangular microchannel with the reactive side at the bottom. The channel is 10 μm wide and 500 μm long. Part of the channel is shown here. (b) Comparison of the numerical results with the entrance and fully developed analytical solutions for $Pe = 50$ and $Da \to \infty$.

developed curve for larger values of x^*. Larger values of Peclet number will result in even better agreement especially in the entrance region. Now that the numerical model is verified, it is used to examine the performance of the three designs presented in the next section.

3.2. Model validation against experimental results

Hybridization kinetics of DNA strands has been tested and reported in [17] for a rectangular microchannel with a reactive spot labelled with specific ligands. The adsorption/desorption kinetics is monitored by fluorescence microscopy. The DNA solution (29 basis pairs of strands) is released at the inlet (shown in Fig. 2(a)). The channel is 10 mm × 1 mm × 10 mm, and the inlet velocity is 1 mm/s. The flow is turned on for 50 min, then turned off for 310 min and again turned on for the rest of the experiment. The size of the reactive spot and the ligand surface concentration are not explicitly mentioned in Ref. [17]. Here, values consistent with those used in other examples of the same reference are applied. The spot is considered to be 4 mm long, and the ligand surface concentration assumed to be 1×10^{-8} mol/m^2. Backward reaction rate is assumed to be negligible as mentioned in [17]. Also, the values of diffusivity (D), forward reaction rate (k_{on}) and inlet concentration (C_0) were obtained in Reference [17] by fitting the numerical method to the experimental data. Here, the same procedure was followed. Fig. 2(b) shows that for the set of variables obtained from the fitting ($D = 7 \times 10^{-11}$ m^2/s, $k_{on} = 30$ m^3/mol/s, $C_0 = 2.9 \times 10^{-6}$ mol/m^3) the numerical curve follows the experimental data very well. The numerical values for the diffusivity and the inlet concentration are found to be the same as those presented in [17]. However, better fitting to the experimental data is obtained using the forward reaction rate presented here ($k_{on} = 30$ m^3/mol/s) than the one mentioned in the reference ($k_{on} = 75$ m^3/mol/s). The two values are still in the same order. The difference may exist due to the discrepancies in the assumed surface concentration or reactive surface configuration.

4. Geometry

Fig. 3 shows the microchannels with three different microreactor geometries considered for the analysis. The geometries are the parallel-plates (PP) open channel, circular micropillars (CM), and screen plates (SP). In all cases, the design criteria that the reactive surface area and the overall channel size must be the same are met. The length of the microchannel is 235 μm, and the height is 120 μm. The total length of the reactive boundary is considered 470 μm for the screen-plate and parallel-plate designs (i.e., same as the reactive length currently being implemented in the flow cell device used by the authors in the laboratory). The plates are assumed to be reactive only at the front side in the screen-plate design. The gap between the plates in the screen-plate design and between the cylinders in the circular-micropillar design is 10 μm, which works

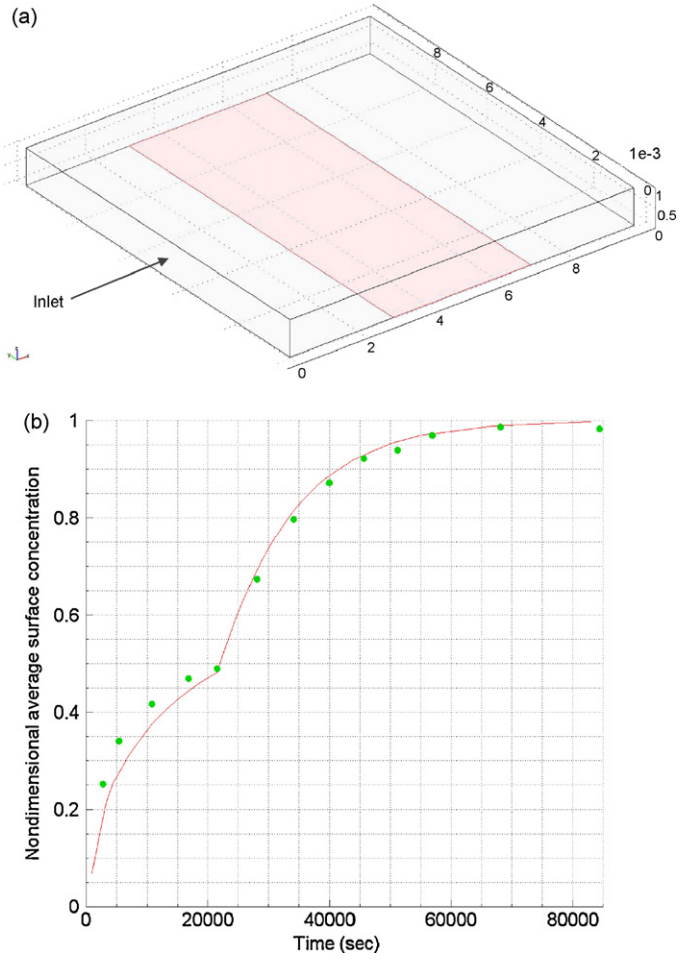

Fig. 2. Validation of the numerical model: (a) rectangular microchannel with the reactive plate shown in red color and (b) fit of the experimental data for 29 basis pairs of DNA strands with the numerical results.

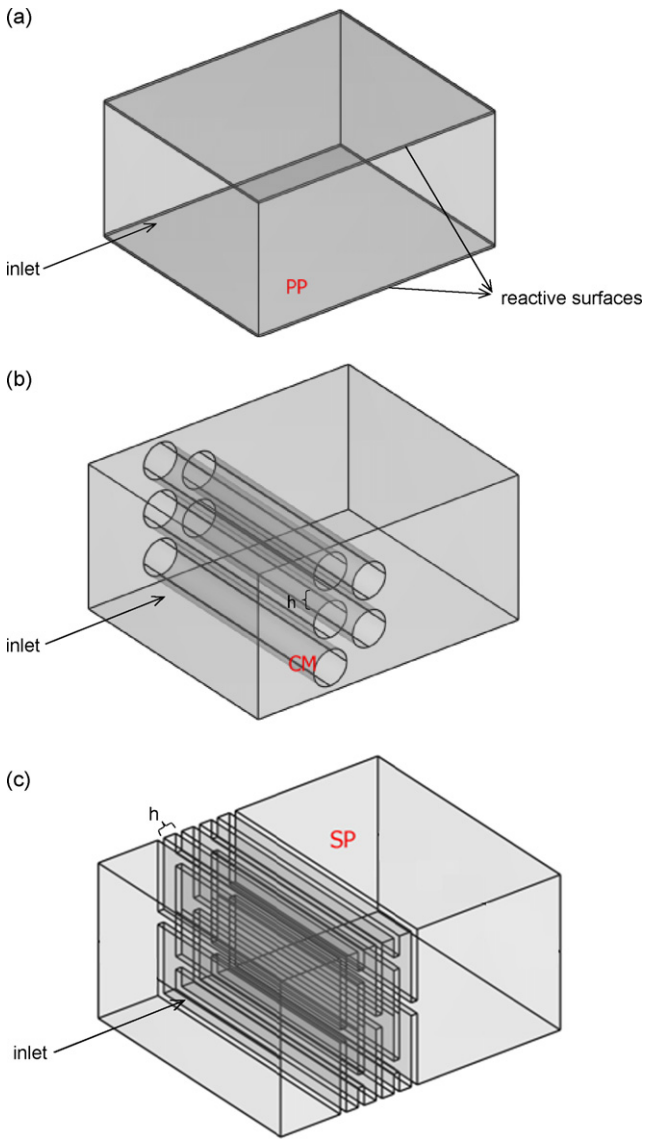

Fig. 3. Geometries of three microreactors: (a) parallel-plate open channel (PP) in which top and bottom surfaces are reactive, (b) circular micropillars (CM) in which cylinder surfaces are reactive and (c) screen plates (SP) in which only front sides of the plates are reactive.

well for biomolecules without causing any clotting. For the circular-micropillar design, the length of the reactive boundary is 471.2 μm since in this case it is not possible to have exactly the same length as the others and keep the flow path width constant at 10 μm. Thus, a length very close to the set value (i.e., 470 μm) is selected. Compared to the numerical error in the simulations, this difference is not expected to have significant influence.

5. Results and discussion

5.1. Device performance comparison

In the following sections, two different parameters, including capture efficiency and average surface concentration adsorbed on the reactive area, are used to carry out the comparison. Capture efficiency is calculated based on [30]

$$CE = 1 - C^*_{b,outlet} \tag{14}$$

Table 1
Numerical values of the parameters used for the simulations in Figs. 6–8 (taken from [35–37]).

Parameter	Value
Forward reaction rate (k_{on})	10^5 m^3/(mol s)
Backward reaction rate (k_{off})	10^{-2} s^{-1}
Ligand concentration (C_{s0})	10^{-8} mol/m^2
Diffusion coefficient (D)	10^{-11} m^2/s
Inlet concentration (C_0)	10^{-6} mol/m^3
Average inlet velocity (u_{avg})	10^{-4} m/s
Peclet number (Pe)	100
Damkohler number (Da)	1000
Relative adsorption capacity (ε)	0.01
Equilibrium dissociation constant (K_D)	0.1

where $C^*_{b,outlet}$ is the non-dimensional form of the bulk concentration at the outlet ($C_{b,outlet}$) and is defined as

$$C^*_{b,outlet} = \frac{1}{C_0 u_{avg} h} \int_0^h C_{outlet} u_{outlet}\, dy \tag{15}$$

Throughout this paper, this parameter is used to find the gain in the adsorbed concentration whenever a design factor is changed and the reactive area is unchanged.

It is clear that increasing the area leads to higher adsorbed concentrations and capture efficiencies. Therefore, there must be another criterion to scale the gain in the adsorbed solute and include the effort made for preparing the reactive surface. To meet this need, average surface concentration, $C_{s,avg}$, is determined. $C_{s,avg}$ is interpreted as the performance of the device and obtained from the following formula for the unit depth of the channel

$$C_{s,avg} = \frac{1}{l} \int_{reactive\ area} C_s\, dx \tag{16}$$

where l is the length of the reactive surface. $C_{s,avg}$ is used whenever the reactive surface area is changed for a device.

Table 1 presents the numerical values of the chemical and physical parameters and the corresponding non-dimensional numbers used for the simulations. These values are within the range observed in common biological reactions [35–37]. COMSOL Multiphysics software is used to solve the governing equations in two steps. First, the Navier-Stokes equations are solved in the domain and the steady-state velocity is obtained. Then, the transient mass transport equation is used along with the kinetic equation to derive the concentration profile of the solute in the bulk and on the surface. Fig. 4 shows how the three geometries introduced in Section 4 are meshed. A triangular mesh is used throughout the domain and is refined near the reactive boundaries to capture the high gradients of concentration. The problem is sensitive to the mesh on the boundaries especially around the edges where the gradients are larger. Throughout this paper, mesh independency is investigated with the margin of 1% change in the numerical results. The buffer liquid with the solute is allowed to flow through the channel for 5 min which is in the range of the usual sampling times. Due to symmetry, only half of each geometry is modeled. The Reynolds numbers investigated here lie in the range of 10^{-5} to 10^{-3} (corresponding to the average velocities between 1 and 100 μm/s) which is in the Stokes flow regime. Fig. 5 depicts the streamlines for two of the geometries (i.e., screen plates and circular micropillars) which are not as straight forward as the parallel-plate design. The streamlines show a laminar flow of solution without forming any vortices in the vicinity of the reactive areas. Figs. 6–8 present sample concentration plots within the domain and on the reactive surfaces for each design. After 5 min, the capture efficiency (CE) is 1.6%, 15.5% and 15.7% for the parallel-plate (PP), circular-micropillar (CM) and screen-plate (SP) designs, respectively. As it is expected, the efficiency significantly improves by changing the design from the open

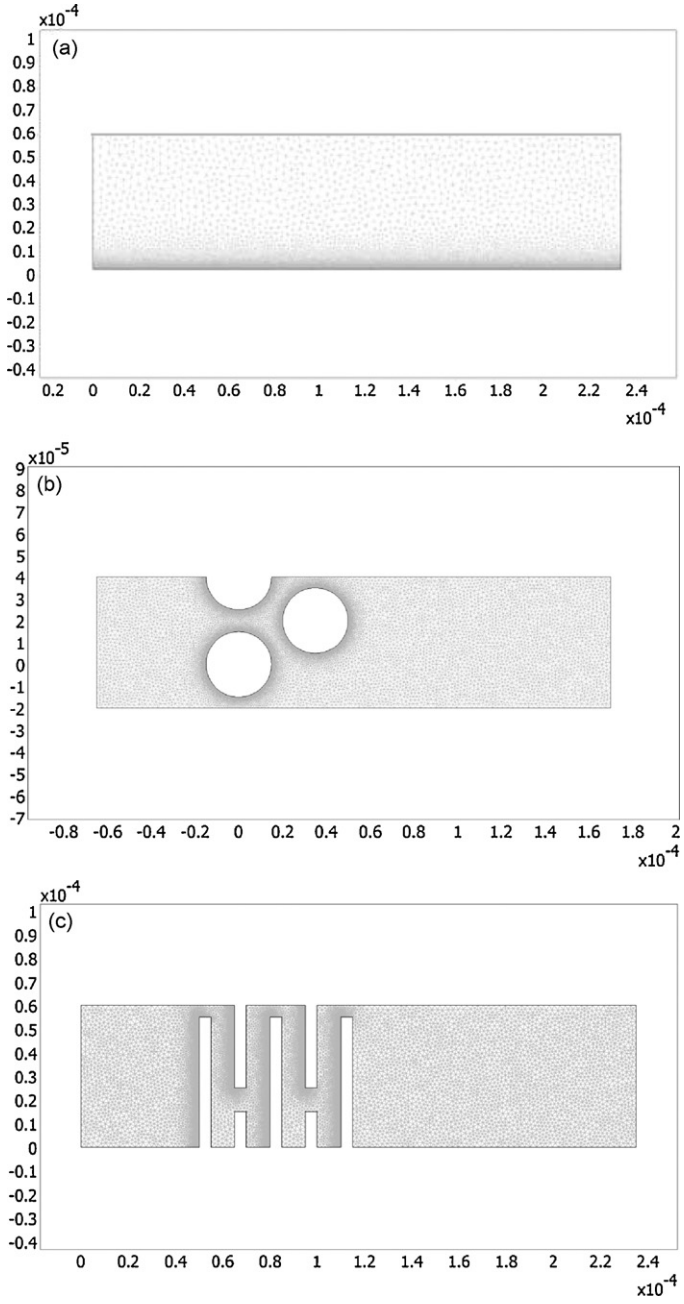

Fig. 4. View of the mesh in: (a) parallel-plate open channel, (b) circular micropillars and (c) screen plates.

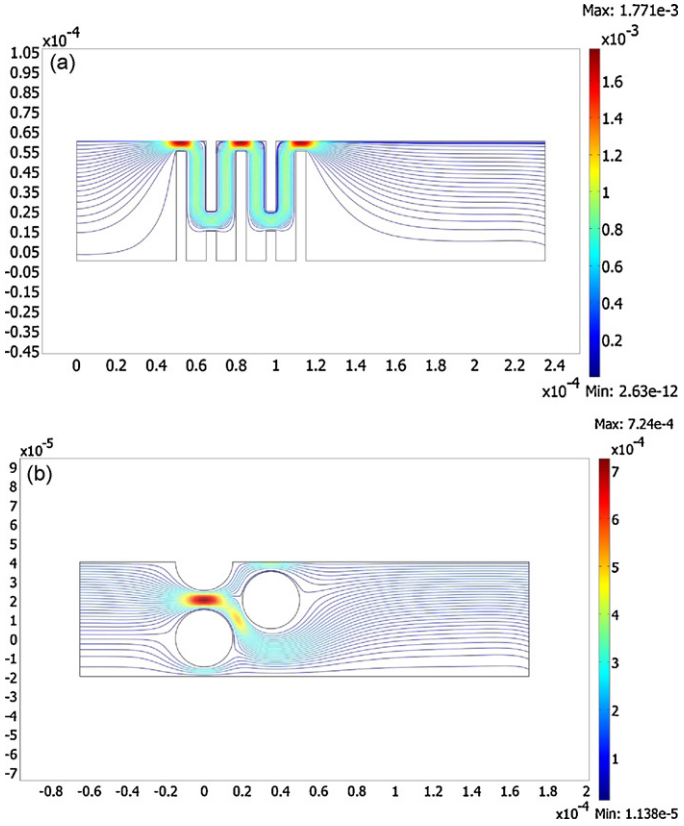

Fig. 5. Streamlines in: (a) circular micropillars and (b) screen plates for $Re = 10^{-3}$. Edge effects are observed at the outlet far from the reactive obstacles.

channel to the packed-bed geometry. However, for the packed-bed designs, there is no significant difference (within the numerical solution error) between the screen plates and the circular pillars. To compare the three designs more accurately, the simulation is conducted for four different Peclet numbers. Damkohler number is kept constant (at 1000), so the problem is in transport-limited regime. This is desirable since the effect of the geometry on the improvement of transport is of interest here. *Pe* is changed because convection and diffusion, as the two mechanisms of dispersion, are of great importance and the corresponding trends reveal the relative importance of each term. Fig. 9 shows the capture efficiency of three different designs versus *Pe* for the reactive lengths of 470 μm. For all the geometries, as *Pe* increases, *CE* decreases since the convection time scale becomes smaller than the diffusion time scale. As a result, biomolecules are carried away by the buffer liquid before they diffuse to the reactive surfaces. Conversely, for smaller *Pe*, biomolecules have enough time to adsorb on the surface. Since the time scale of reaction is short (high *Da*), very large capture efficiency are gained for small *Pe*.

From Fig. 9, the capture efficiencies for the two packed-bed configurations (i.e. the screen plates and the circular pillars) are found to be significantly larger than the capture efficiency of the parallel plates. This improvement is due to the significant reduction in the diffusion path of the solute in the bulk and also the effect of convection. The ratio of the capture efficiency of PP design to SP (or CM) design monotonically increases from around 1.4 to 10 as *Pe* number increases from 1 to 100. So, the relative gain seems to be more considerable for higher Peclet numbers.

To gain a better insight into the results obtained here, two parameters are introduced: the diffusion time (i.e., the time necessary to transport a biomolecule to the reactive surface through diffusion) and the convection time (i.e., the time within which a biomolecule travels through the reactive domain). These two times are defined as

$$t_d = \frac{l_d^2}{4D} \tag{17}$$

$$t_c = \frac{l}{U} \tag{18}$$

in which l_d is the diffusion path which is assumed to be half of the gap between the reactive surfaces, l is the total length that a biomolecule is traveling close to a reactive surface inside the reactive box, U is assumed to be the maximum flow velocity in the device, and D is the diffusion constant. These parameters provide a rough estimate of the diffusion and convection times for a biomolecule which is moving in the middle of the gap between the reactive plates. The ratio of these two times (t_c/t_d) determines the relative capacity of the device to capture that biomolecule.

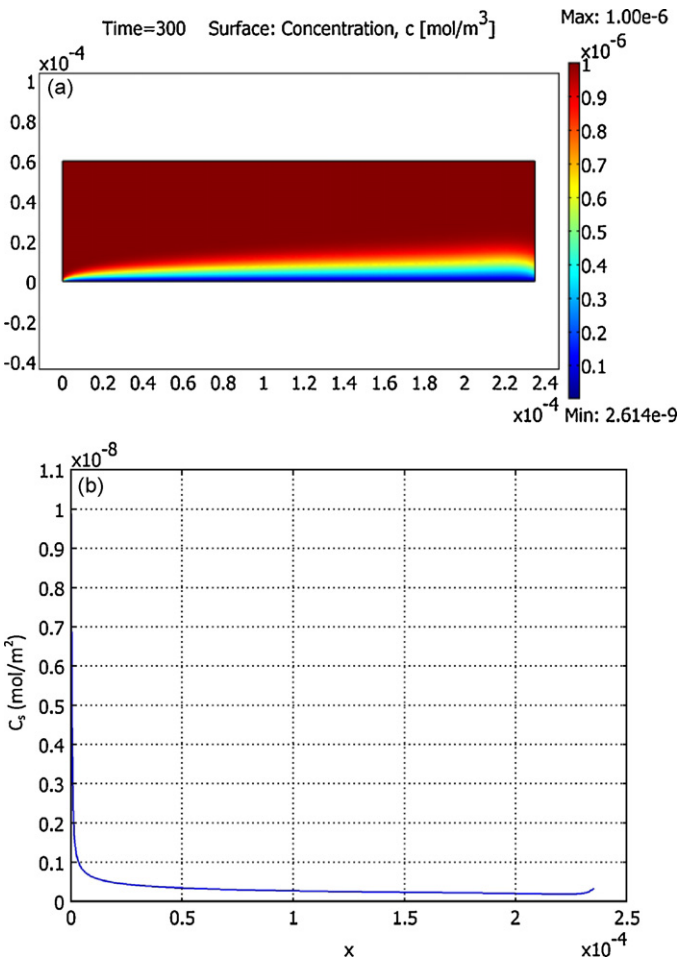

Fig. 6. Concentration plot: (a) in the bulk and (b) on the reactive surface.

Larger values are favourable since they indicate smaller time scales of diffusion and larger efficiencies. For instance, for $Re = 10^{-3}$ and $Pe = 100$, this ratio (t_c/t_d) is approximately 0.02, 0.1 and 0.12 for parallel plates, circular pillars and screen plates, respectively. Comparing these values demonstrates the relative superiority of the packed-bed design with respect to the open channel.

The comparison between the capture efficiencies of SP and CM designs shows that their performances are almost indistinguishable (see Fig. 9). Considering the numerical error in the simulation, it is concluded that there is no significant gain in changing the design from the screen plates to the circular micropillars. Fabrication process may be the same in terms of difficulty for SP and CM designs. However, screen plates greatly facilitate the process of the immobilization of the antibodies and also the detection of the deposited biomolecules on the reactive surfaces. Considering the good performance and ease of implementation, screen-plate design is a favourable option to use in the biomolecule separation process in the laboratory. In the next section, this configuration is analyzed in terms of the effect of the design parameters.

5.2. Analysis of the screen-plate design

This section investigates the influence of the physiochemical design parameters and the geometric design parameters (including the number of the plates and reactive side preference) on the output of the biomolecule separation process for the screen-plate reactor selected in the previous section. The effects of physiochemical parameters are analyzed in terms of the non-dimensional factors presented in Section 2.3.

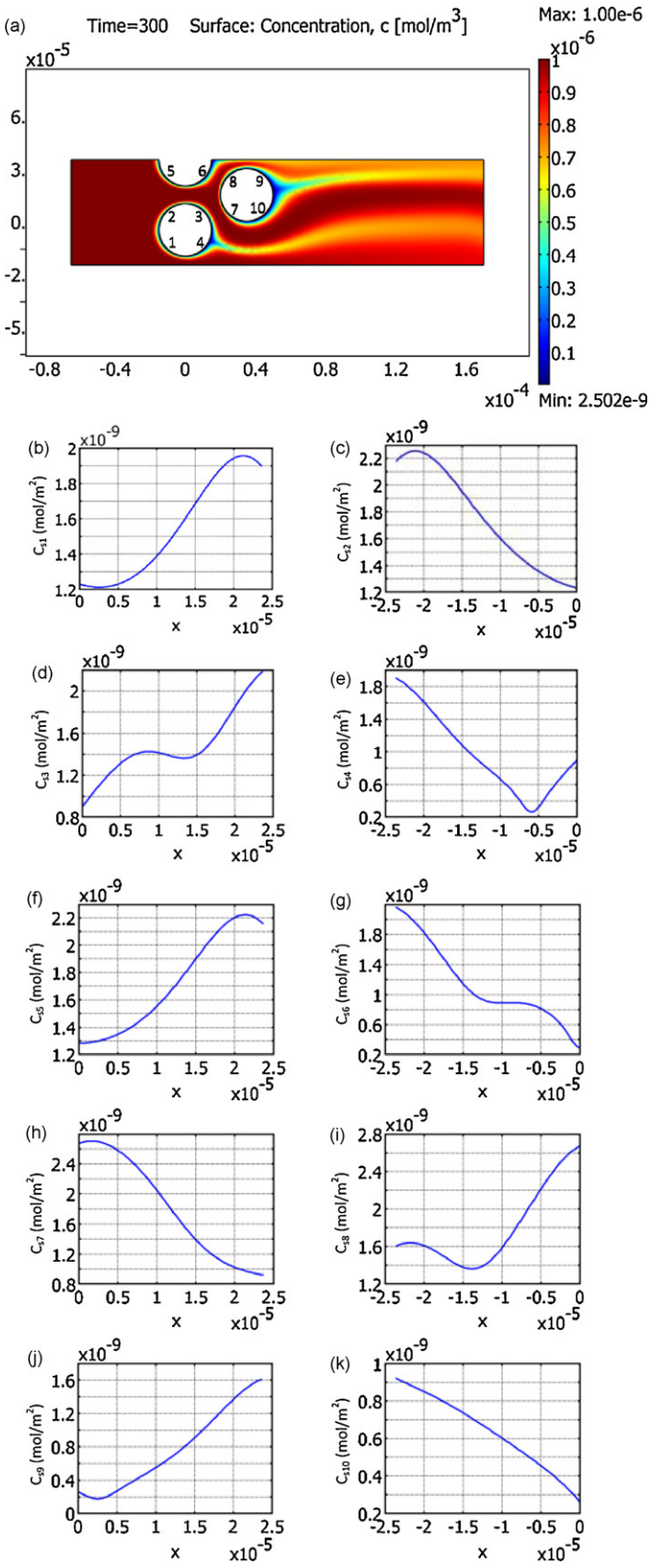

Fig. 7. Concentration plots: (a) in the bulk and (b–k) on the reactive surfaces for $Pe = 100$, $Da = 1000$, $K_D = 0.1$ and $\varepsilon = 0.01$. Each reactive surface is a quarter of a circle numbered in Fig. 4(a).

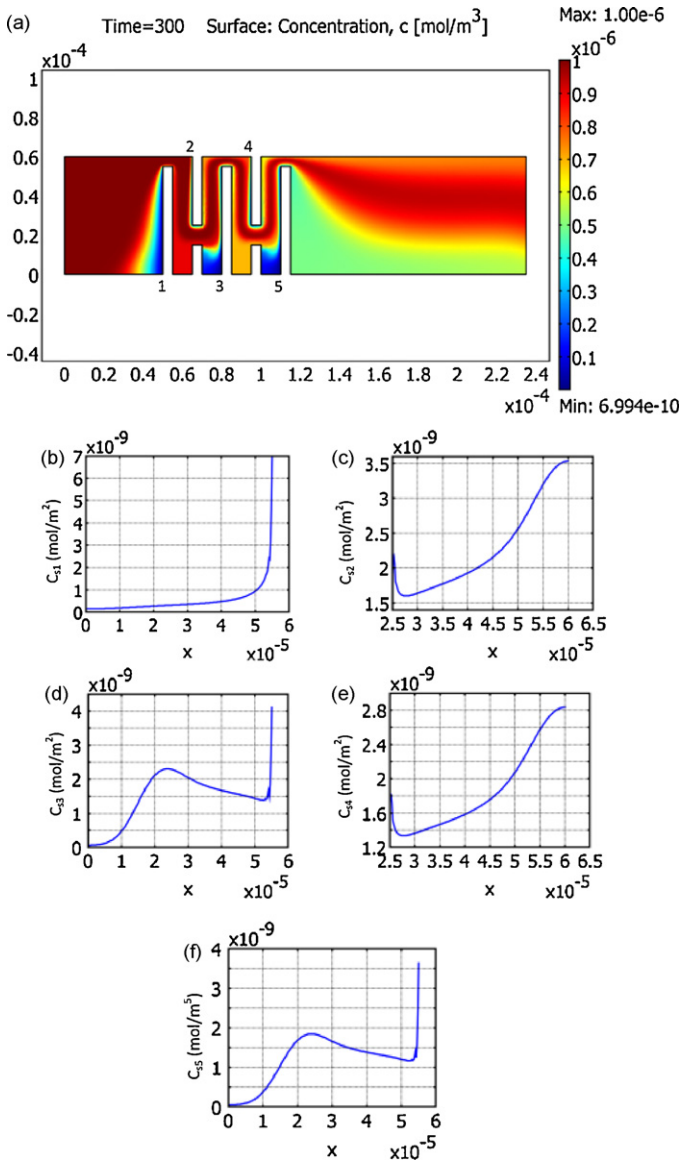

Fig. 8. Concentration plots: (a) in the bulk and (b–f) on the reactive surfaces for $Pe = 100$, $Da = 1000$, $K_D = 0.1$ and $\varepsilon = 0.01$. Only front sides are reactive.

5.2.1. Physiochemical parameters

Biomolecules differ in their affinity to bind to each other. Different types of ligands result in different values of the forward and backward reaction rates [36–38]. Also, they may have different diffusivities in different solutions used for in vitro experiments. For instance, the diffusion coefficient for protein A33 used in immunoassay study is around $10^{-10}\,m^2/s$ while it is around $4 \times 10^{-11}\,m^2/s$ for DNA [30]. All the physiochemical parameters are combined in the four non-dimensional numbers introduced in Section 2.3 to simplify the analysis. Among these four numbers, Damkohler and Peclet numbers are of great importance as they represent the relative strengths of reaction, convection and diffusion once the type of reactants, the ligand surface density and the inlet concentration is known. Fig. 10 depicts the trend of the capture efficiency (CE) versus Damkohler number for three different values of Peclet number (keeping ε and K_D constant) for the time that bulk concentration has reached its steady state. It is shown that, for any specific Pe, the capture efficiency generally increases as Da increases. However, the rate of increase is less for larger Da since the process has shifted to the transport-limited regime ($Da \to \infty$)

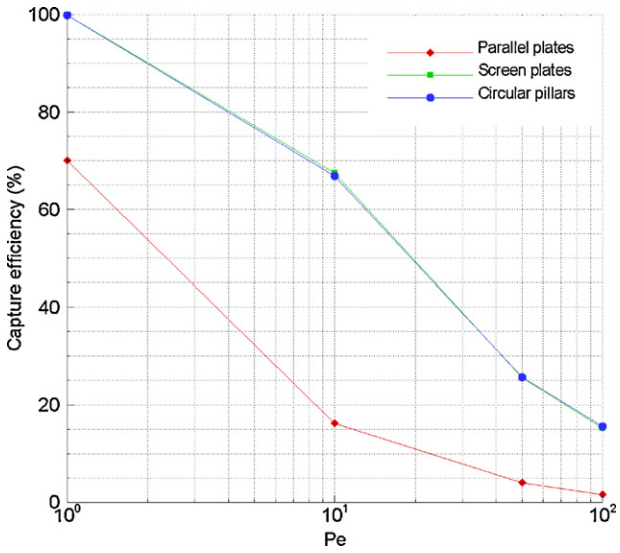

Fig. 9. Capture efficiency versus Peclet number for different designs with reactive length = 470 μm, $Da = 1000$, $K_D = 0.1$ and $\varepsilon = 0.01$.

and higher strength of reaction (with constant diffusivity) does not improve the efficiency very much. This explains the plateau on the right part of the plots. In addition, Fig. 10 shows that for any specific Da, decreasing Pe augments the efficiency. This behaviour was also observed in the previous section where different designs were compared for $Da = 1000$ (Fig. 7). It is worth mentioning that in all the plots throughout the paper, whenever the efficiency approaches to very small values (lower than 1%), the results are not accurate because of the numerical error margin considered.

5.2.2. Number of reactive units

An interesting geometric study in the screen-plate design can be the investigation of the effect of the number of reactive plates on the performance of the device. Since the reactive area is changed in this case, the average surface concentration is plotted to scale the gain obtained by adding the plates. Fig. 11 presents the non-dimensional average surface concentration, $C^*_{s,avg}$, versus the number of units. Each reactive unit consists of two screen plates positioned consecutively. This is shown in the top right part of the figure. Changing

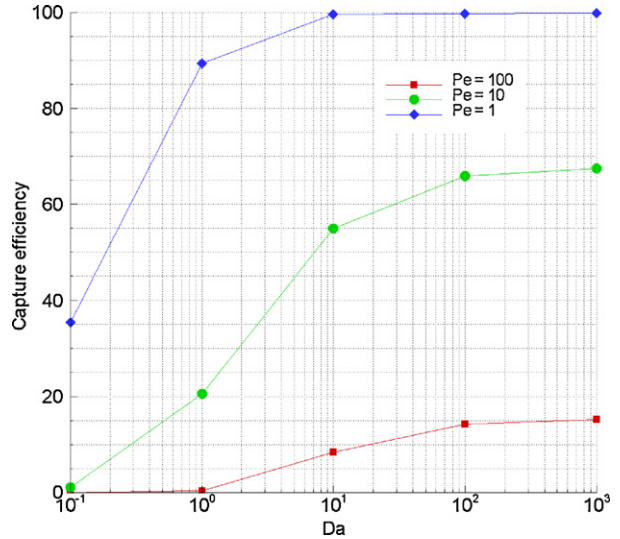

Fig. 10. Capture efficiency of screen plates versus Da number for different Pe numbers ($K_D = 0.1$ and $\varepsilon = 0.01$).

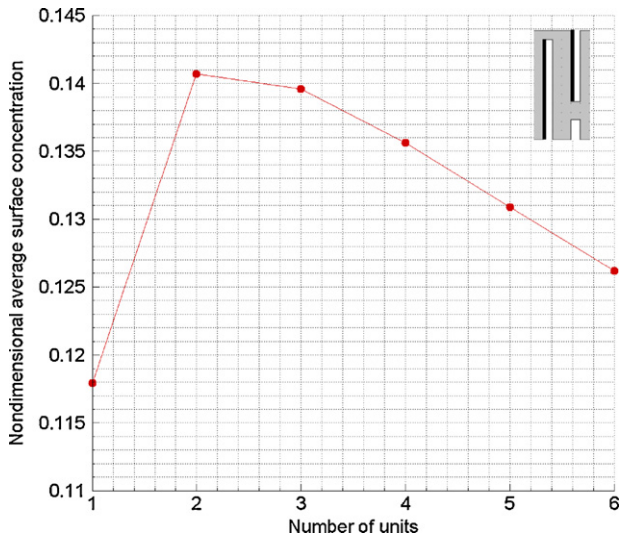

Fig. 11. Non-dimensional average surface concentration versus number of reactive units for $Pe = 100$, $Da = 1000$, $K_D = 0.1$ and $\varepsilon = 0.01$. The single unit shown on the top right part of the plot includes two plates reactive on the front side.

the number of units from 1 to 2 enhances the average adsorbed concentration. However, $C^*_{s,avg}$ drops continuously afterwards. It means that despite the gain in the adsorbed surface concentration, the scaled performance of the device (i.e., surface concentration per area) decreases for higher surface areas. Close look at the front side of the first reactive plate in the first unit demonstrates its low capacity to capture biomolecules (for example, see Fig. 8(b)). This capacity significantly improves from this side to the front side of the first reactive plate in the second unit and changes less significantly from the second unit to the third one and so on (compare the areas under the curves in Fig. 8(b), (d) and (f)). In other words, the small increase in the surface concentration because of adding downstream units (after the second unit) does not compensate the increase in the reactive area. Hence, the ratio, which is the average surface concentration, decreases. This explains why the performance is higher for two units than one unit, and is successively lower for larger unit numbers.

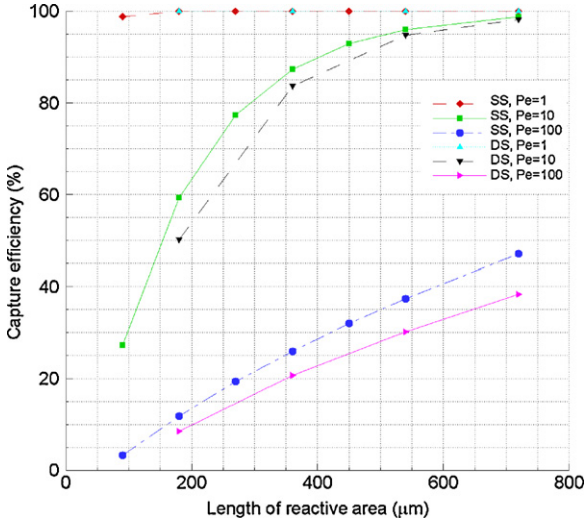

Fig. 12. Capture efficiency versus length of the reactive surface for the single-sided and double-sided devices for different Peclet numbers ($Da = 1000$, $K_D = 0.1$ and $\varepsilon = 0.01$).

5.2.3. Double-sided reactive surfaces

While fabricating the device, either side or both sides of the plates can be labelled depending on the experimental conditions. Although the double-sided reactive plates have the advantage of providing the same reactive area within a smaller device, the capture efficiency is the main criterion to select the configuration. In this paper, alternative configurations have been studied to find the one which has the highest capture efficiency for the same reactive area. Fig. 12 shows the capture efficiency for single-sided (SS) and double-sided (DS) devices with different reactive lengths at three Peclet numbers. This figure reveals the fact that for all the range of reactive areas investigated here, the double-sided design has lower capture efficiency compared to the single-sided design. For lower Peclet numbers (smaller diffusion time scale), the efficiencies are very close since the dominant mechanism (diffusion) works equally for both designs. As Peclet number increases, the difference between efficiencies is more significant. Thus, convection is more influential when the reactive areas are fabricated single-sided against the flow.

6. Conclusions

Microfluidic devices with flow-through channels and mass transport to reactive surfaces have drawn attentions in recent chemical and biological studies. Since the biomolecular reactions take place at the surfaces, finding the optimal device configuration to capture as many biomolecules as possible on the surface is a crucial step in the design process. The determination of the optimal configuration as well as the best range of working condition is very complicated due to the large number of the parameters governing the physics of the problem. The numerical model introduced in this paper enables the researcher to compare the performance of alternative assemblies of the same reactive area inside a fixed volume. Packed-bed designs (including screen plates and circular micropillars) were proved to enhance significantly the reaction performance over the conventional open-channel reactors. This is a direct result of reducing the diffusion path and using convection in biomolecule transport. The increase in the capture efficiency is more significant when the Peclet number is larger. The only small drawback is the larger pressure drop across the channel. For example, for $Re = 10^{-3}$, the pressure drops are around 0.054, 1.8 and 22 Pa for parallel plates, circular pillars and screen plates, respectively. This is expected due to the fact that the screen plates are bluff bodies. The numerical model presented here also allows the thorough examination of the effect of design parameters on the device efficiency. The screen-plate design was selected in this paper to do the parametric study due to good performance and ease of fabrication. It was shown that adding to the number of reactive plates does not generally increase the scaled performance (average surface concentration) of the device. In addition, labelling reactive surfaces on both sides was found to decrease the capture efficiency of the device compared to the single-sided reactive surfaces. This decrease is more considerable for larger Peclet numbers. Different regimes (such as transport-limited regime and reaction-limited regime) were also observed when physiochemical parameters were changed over their usual ranges in biochemical reactions. Recognizing these regions can be useful to find out where the experiment conditions lie and how to adjust them since some changes to the parameters do not significantly contribute to the output and are worth neither the effort nor the cost.

References

[1] S.J. Lee, S.Y. Lee, Micro total analysis system (μ-TAS) in biotechnology, Appl. Microbiol. Biotechnol. 64 (2004) 289–299.

[2] D.J. Beebe, J.S. Moore, Q. Yu, R.H. Liu, M.L. Kraft, B. Jo, C. Devadoss, Microfluidic tectonics: a comprehensive construction platform for microfluidic systems, Proc. Natl. Acad. Sci. U.S.A. 97 (2000) 13488–13493.
[3] T. Chován, A. Guttman, Microfabricated devices in biotechnology and biochemical processing, Trends Biotechnol. 20 (2002) 116–122.
[4] H.A. Stone, A.D. Stroock, A. Ajdari, Engineering flows in small devices: microfluidics toward a lab-on-a-chip, Annu. Rev. Fluid Mech. 36 (2004) 381–411.
[5] G.M. Whitesides, The origins and the future of microfluidics, Nature 442 (2006) 368–373.
[6] L. Kiwi-Minsker, A. Renken, Microstructured reactors for catalytic reactions, Catal. Today 110 (2005) 2–14.
[7] N. Nguyen, S.T. Wereley, Fundamentals and Applications of Microfluidics, Artech House, Norwood, 2006.
[8] P. Auroux, D. Iossifidis, D. Reyes, A. Manz, Micro total analysis systems. 2. Analytical standard operations and applications, Anal. Chem. 74 (2002) 2637–2652.
[9] L.R. Snyder, J.J. Kirkland, J.W. Dolan, Introduction to Modern Liquid Chromatography, John Wiley & Sons, New Jersey, 2010.
[10] D.S. Hage, Affinity chromatography: a review of clinical applications, Am. Assoc. Clin. Chem. 45 (1999) 593–615.
[11] J.M. Brockman, B.P. Nelson, R.M. Corn, Surface plasmon resonance imaging measurements of ultrathin organic films, Annu. Rev. Phys. Chem. 51 (2000) 41–63.
[12] P. Schuck, Use of surface plasmon resonance to probe the equilibrium and dynamic aspects of interactions between biological macromolecules, Annu. Rev. Biophys. Biomol. Struct. 26 (1997) 541–566.
[13] Y. Okahata, M. Kawase, K. Niikura, F. Ohtake, H. Furusawa, Y. Ebara, Kinetic measurements of DNA hybridisation an oligonucleotide-immobilized 27-MHz quartz crystal microbalance, Anal. Chem. 70 (1998) 1288–1296.
[14] T.P. Burg, S.R. Manalis, Suspended microchannel resonators for biomolecular detection, Appl. Phys. Lett. 83 (2003) 2698–2700.
[15] R.D. Oleschuk, L.L. Shultz-Lockyear, Y. Ning, D.J. Harrison, Trapping of bead-based reagents within microfluidic systems: on-chip solid-phase extraction and electrochromatography, Anal. Chem. 72 (2000) 585–590.
[16] P. Tabeling, Introduction to Microfluidics, Oxford University Press, New York, 2005.
[17] J. Berthier, P. Silberzan, Microfluidics for Biotechnology, 2nd ed., Artech House, Norwood, 2010.
[18] G. Taylor, Dispersion of soluble matter in solvent flowing slowly through a tube, Proc. R. Soc. Lond. A 219 (1953) 186–203.
[19] R. Aris, On the dispersion of a solute in a fluid flowing through a tube, Proc. R. Soc. Lond. A 235 (1956) 67–77.
[20] M. Pagitsas, A. Nadim, H. Brenner, Projection operator analysis of macrotransport processes, J. Chem. Phys. 84 (1986) 2801–2807.
[21] G.N. Mercer, A.J. Roberts, A center manifold description of contaminant dispersion in channels with varying flow properties, SIAM J. Appl. Math. 50 (1990) 1547–1565.
[22] R. Sankarasubramanian, W.N. Gill, Unsteady convective diffusion with interphase mass transfer, Proc. R. Soc. Lond. A 333 (1973) 115–132.
[23] N.G. Barton, An asymptotic theory of dispersion of reactive contaminant in parallel flow, Aust. Math. Soc. B 25 (1984) 287–310.
[24] M. Shapiro, H. Brenner, Taylor dispersion of chemically reactive species: irreversible first order reactions in bulk and on boundaries, Chem. Eng. Sci. 41 (1986) 1417–1433.
[25] D. Dutta, A. Ramachandran, D.T. Leighton Jr., Effect of channel geometry on solute dispersion in pressure-driven microfluidic systems, Microfluid. Nanofluid. 2 (2006) 275–290.
[26] D. Dutta, D.T. Leighton, Dispersion reduction in pressure-driven flow through microetched channels, Anal. Chem. 73 (2001) 504–513.
[27] Ch.N. Baroud, F. Okkels, L. Ménétrier, P. Tabeling, Reaction–diffusion dynamics: confrontation between theory and experiment in a microfluidic reactor, Phys. Rev. A 67 (2003) 060104.
[28] H. Wang, P. Iovenitti, E. Harvey, S. Masood, Optimizing layout of obstacles for enhanced mixing in microchannels, Smart Mater. Struct. 11 (2002) 662–667.
[29] N. Aoki, Sh. Hasebe, K. Mae, Geometric design of fluid segments in microreactors using dimensionless numbers, AIChE J. 52 (2006) 1502–1515.
[30] T. Gervais, K.F. Jensen, Mass transport and surface reactions in microfluidic systems, Chem. Eng. Sci. 61 (2006) 1102–1121.
[31] A.N. Waghode, N.S. Hanspal, I.M.T.A. Shigidi, V. Nassehi, K. Hellgardt, Computer modelling and numerical analysis of hydrodynamics and heat transfer in non-porous catalytic reactor for the decomposition of ammonia, Chem. Eng. Sci. 60 (2005) 5862–5877.
[32] E. Papoutsakis, D. Ramkrishna, Conjugated Graetz problems. 1. General formalism and a class of solid-fluid problems, Chem. Eng. Sci. 36 (1981) 1381–1391.
[33] S. Usami, H. Chen, Y. Zhao, S. Chien, R. Skalak, Design and construction of a linear shear stress flow chamber, Ann. Biomed. Eng. 21 (1993) 77–83.
[34] L.L. Munn, R.J. Melder, R.K. Jain, Analysis of cell flux in the parallel plate flow chamber: implications for cell capture studies, Biophys. J. 67 (1994) 889–895.
[35] M.B. Lawrence, T.A. Springer, Leukocytes roll on a selection at physiologic flow rates: distinction from and prerequisite for adhesion through integrins, Cell 65 (1991) 859–873.
[36] D.A. Hammer, D.A. Lauffenburger, A dynamical model for receptor-mediated cell adhesion to surfaces, Biophys. J. 52 (1987) 475–487.
[37] G. Bell, M. Dembo, P. Bongrand, Cell adhesion: competition between nonspecific repulsion and specific bonding, Biophys. J. 45 (1984) 1051–1064.
[38] G. Bell, Models for the specific adhesion of cells to cells, Science 200 (1978) 618–627.